JOURNAL OF GEOPHYSICAL RESEARCH, VOL. 106, NO. B5, PAGES 8687–8698, MAY 10, 2001

Comparison of the microfracture localization in granite between fracturation and slip of a preexisting macroscopic healed joint by acoustic emission measurements

Laurence Jouniaux

École Normale Supérieure de Paris, Unité Mixte de Recherche 8538, CNRS, Paris, France

Koji Masuda, Xinglin Lei, Osamu Nishizawa, and Kinichiro Kusunose

Geological Survey of Japan, Tsukuba, Japan

Liqiang Liu and Wentao Ma

China Seismological Bureau, Beijing, China

Abstract. Experiments of fracturation and slip of a preexisting macroscopic healed joint have been performed under triaxial deformation on granite from Mayet de Montagne (France). This granite shows high grain-scale inhomogeneity. Acoustic emissions have been recorded and hypocenters have been determined during the entire experiments. For both rupture experiment and slip experiment, precursory localization of microfractures in the final rupture plane has been observed in the early stage of deformation, well before the dilatancy. It is likely that not only initial closure of favorably oriented cracks but also breaking of partially cemented grains or slipping between grains may occur in the pseudoelastic phase and are already localized on the final rupture plane where the shear stress seems to be concentrate. This behavior is observed in both cases where stress heterogeneity and rupture nucleation are controlled by (1) medium-scale heterogeneity at the grain scale (HS sample) or (2) macroscopic heterogeneity in the form of a preexisting healed joint (JS sample). The sample with the healed joint exhibited ~ 1.6 times more acoustic emission events than the intact sample. The presence of the healed joint significantly weakened the sample.

1. Introduction

It is usually accepted that faulting of brittle rocks is induced by coalescence of microcracks formed prior to faulting. These microcracks are initially randomly distributed and subparallel to the maximum compressive stress [*Brace et al.*, 1966], and the coalescence occurs near the peak stress. During the linear part of the rock deformation, minerals distort elastically and grains or part of grains shift slightly under the applied stress and slide relative to one another [*Brace et al.*, 1966]. Microcracks deform or close depending on their orientations. However, new cracks appear at preexisting intergranular at the onset of volume increase and then at 50-75% of peak stress new transgranular cracks appear [*Tapponier and Brace*, 1976; *Fonseka et al.*, 1985]. The growth of microcracks is associated to mismatch of grain boundaries, differences in elastic moduli between minerals, intracrystalline flaws, and shear along grain boundaries [*Taponnier and Brace*, 1976]. Model for the deformation and failure of brittle rock has been developed from the mechanics of tensile microcracks [*Costin*, 1983; *Main*, 1991]. Another model of failure of brittle solids has been developed considering crack initiation, crack propagation, and crack linkage [*Nemat-Nasser and Horii*, 1982; *Ashby and Hallam*, 1986]. Both axial and shear cracks play significant roles in the faulting process; small cracks grow stabily until their length is comparable with their spacing. When they interact, an instability develops to give final failure [*Ashby and Sammis*, 1990], and at later stages of deformation, extensive crushing of particles into fine-grained fault gouge is important [*Wong*, 1982].

In this paper we describe two experiments of rock deformation under triaxial stress up to fracture strength on two granite samples: an intact sample (HS), and a sample having a preexisting macroscopic healed joint (JS) from the bottom to the top of the sample with an angle of ~20° to the axial direction and ~ 1 mm in aperture. Therefore the JS sample is constrained to have a fracture running from the top to the bottom of the sample. Note that these samples have different grain sizes and are not as homogeneous as material usually used in other experiments. The preexisting healed joint was thought to control the rupture initiation. This healed joint was expected to slip during the deformation or the final stage of deformation. However, it was not known if this healed joint acts as strong or weak component, depending on the nature and degree of cementation. Acoustic emission (AE) were observed by counting the cumulative number and by determinating the source location.

One goal of our experiments was to know if the eventual rupture plane would appear earlier in the loading history by showing an increased and localized AE activity, when a preexisting joint exists. Samples were loaded up to failure, and

Paper number 2000JB900411.
0148-0227/01/2000JB900411$09.00

since brittle fracture involves the growth of microcracks, acoustic signals were spontaneously generated from this microcracking. Indeed, AE are high-frequency elastic waves generated by the localized relaxation of stress or displacement as a local dislocation or by crack propagation. Note that the observed AE are probably the result of unstable crack propagation, meaning rapid microcrack growth [*Lockner*, 1993]. The microcrack damage is anisotropic and AE source location can detect the three-dimensional distribution of microfractures. We address the question of when the macroscopic fracture plane can be first identified from AE locations when an intact sample is fractured and when a slip occurs on a preexisting healed joint.

2. Experimental Setup

Two samples of granite from Mayet de Montagne (France) were cut into cylinders of 100 mm length by 50 mm diameter. This granite contains quartz (1 to 5 mm diameter), K-feldspar (grains up to 3 cm diameter), biotite, and muscovite (1 to 3 mm diameter) hornblende. The grain size to sample ratio for the largest quartz grains is therefore ~ 0.1, which is large compared to other experiments described in the literature. Images of the intact samples were made under X-ray tomography, one cross section each millimeter being scanned. The same procedure was used after the experiments in order to see the fracture using a nondestructive method. The first sample was an intact sample (HS), and the second sample contained a preexisting throughgoing macroscopic joint (JS). This macroscopic joint contains calcite, prehnite and fluorine [*Clavaud et al.* , 2000]. Flat areas ~ 1 cm in width were ground on the cylindrical surface at 60° intervals around the circumference in order to glue the piezoelectric transducers (PZT). PZT transducers function not only as receivers of acoustic signals but also as acoustic sources. Eighteen PZT transducers (2 MHz resonant frequency, 5 mm in diameter) were used for acoustic emission (AE) detection, six for *P* wave velocity measurements and four to eight for *S* wave velocity measurements. The elastic wave velocities in the axial and radial directions were measured during the experiment by exciting the appropriate piezoelectric sensors (PZT 19 and 20 measured vertical *P* wave, PZT a and 1, b and 2, measured horizontal *P* wave, see Figures 1a and 1b) with a pulse generator, and AE events that occurred during the velocity measurements could not be detected. Velocity measurements were performed for each 25 MPa increment of axial stress during the first part of the experiment, then for each 50 MPa because of the real-time results of velocity measurements. This provided the velocity values used for the AE hypocenter determination.

Six cross-strain gauge pairs, each 6 mm length, were cemented to the sample surface with epoxy resin to measure the local strains at the central portion of the sample (A, B, C, D, E and F in Figure 1). After the gauges and the transducers were glued on the sample, the stainless steel end pieces were attached to each end of the sample. Then the sample and the end pieces were coated with several layers of silicon rubber in order to isolate the sample from the oil used as the fluid-confining pressure medium. The sample assembly was then fixed to the base of a pressure vessel, and all electric leads were connected (with shield wires for each AE sensor) and tested. The pressure vessel was placed in a servocontrolled loading frame and the confining pressure tubing connecting to the pump. After all gauges and PZT were connected to the data acquisition system, uniformity of the axial loading was checked from strain gauge

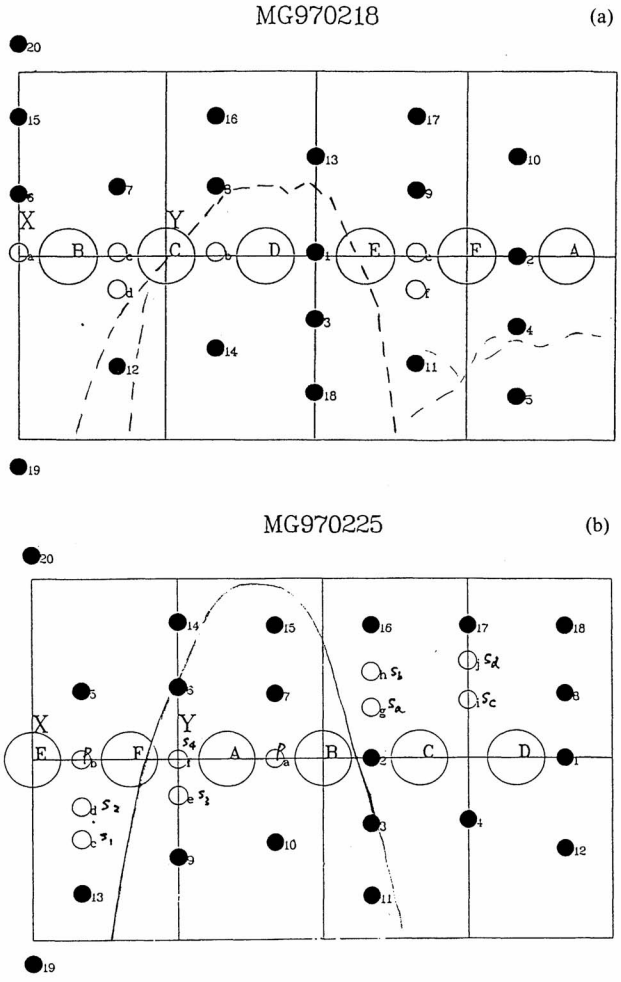

Figure 1. Sample scheme with strain gauges (large circles A to F) and transducers (small circles) locations. Length of sample is 100 mm, and circumference of sample is 314 mm. Transducers 19 and 20 are located on the ends of the sample. Scheme for (a) HS sample and (b) JS sample. The line on Figure 1b represents the location of the healed joint, and dashed line on Figure 1a represents the finale rupture.

outputs. The confining pressure was set at 40 MPa and was held constant thoughout the experiment. The loading rate was 0.052 MPa/s.

3. Data Acquisition System

One data acquisition system collected the values of axial load, confining pressure, strain gauges outputs, and AE counts. No measurements were performed with a smaller time period than 40 s. Another data acquisition system was used to detect, digitize, and store the AE waveforms and elastic waveforms from the transducers. This system is based on the one detailed by *Satoh et al.* [1987] and has been improved [*Nishizawa*, 1997; *Satoh and Nishizawa*, 1997; *Lei et al.*, 1997]. The system digitizes the waveform at a rate of 20 MHz for each channel, for as many as 32 channels. AE hypocenters were determined automatically by picking the first arrival of the *P* wave [*Yokota et al.*, 1981; *Satoh et al.*, 1987; *Masuda et al.*, 1990]. The method calculating AE hypocenters is basically the same as that one used for seismic

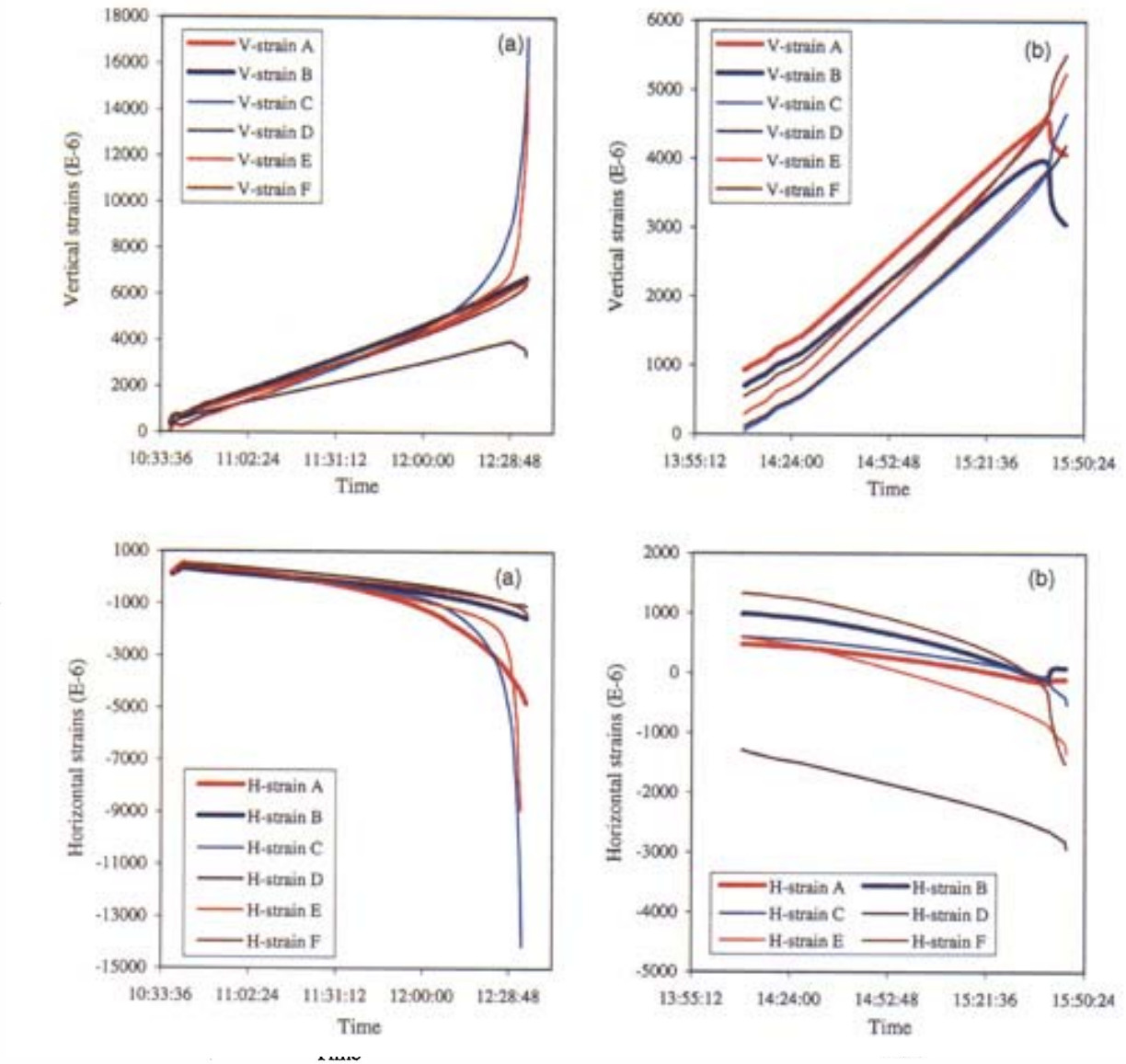

Plate 1a. Vertical and horizontal strains measured from the six different strain gauges for HS sample.

Plate 1b. Same as Plate 1a except for JS sample. Different behavior from strain gauges A and B can be observed.

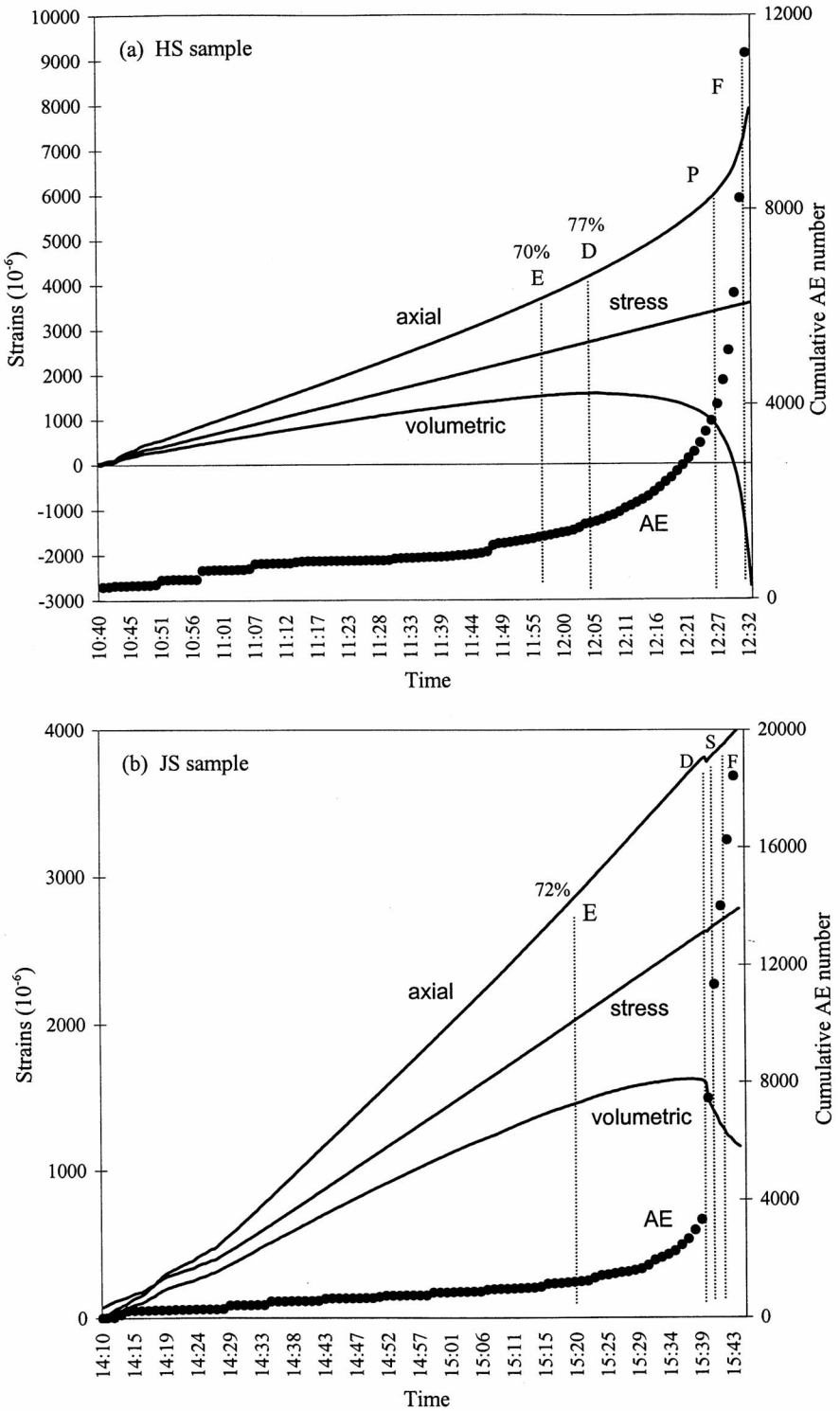

Figure 2. Differential stress, axial strain, volumetric strain evolution and AE cumulative number during the triaxial compression for (a) HS sample and (b) JS sample. Stress is in 10^5 Pa on the axis of strains. E is the end of the linear part in differential stress-vertical strain curve, D is the beginning of increasing volumetric strain, and S is the slip.

events. Those AE hypocenters determined within an error smaller than 2 mm were selected for plotting. Several hypocenters are located outside the sample because of poor conditions for convergence when events occur close to the surface. Thus the results are more accurate within the sample but not too close to the sample boundaries.

4. Results

4.1. Mechanical Behavior

The strain gauges responses during the experiment are plotted in Plates 1a and 1b. The vertical and volumetric strains, the differential stress (axial stress minus confining pressure), and the

Table 1. Mechanical Characteristics for the Homogeneous Sample (HS) and the Sample With a Joint (JS)[a]

Sample	Strength, MPa	*E*, GPa	ν	$\mu = \tau / \sigma_n$
HS	358	67.2	0.32	1.12
JS	278	69.2	0.28	1.22

[a] *E* is the Young'modulus, ν is the Poisson ratio, and μ is the friction (τ / σ_n).

AE cumulative number are shown in Figures 2a and 2b. The strength of HS sample was larger than the one of JS sample (Table 1), showing that the sample of the same material, but with the preexisting joint, was weaker than the intact sample. The deformation (differential stress-vertical strain curve) is linear up to 70% and 72% of strength (E point) for HS and JS sample, respectively. The Young's modulus *E* and the Poisson ratio ν have been deduced from the linear part of the differential stress-vertical strain curve (Table 1).

For the linear deformation part the imposed loading rate induced vertical strain rates of 8.1×10^{-7} s^{-1} and 7.6×10^{-7} s^{-1} for HS and JS samples, respectively, and horizontal strain rates of 2.6×10^{-7} s^{-1} and 2.1×10^{-7} s^{-1} for HS and JS samples, respectively. The maximum vertical shortening was 0.8% and 0.4% for HS and JS samples, respectively.

The HS sample exhibits a typical volumetric change during the deformation; volume decreases by 0.16% during the first 86 min of the experiment (up to point D), and then volume increases by 0.43% at the onset of dilatancy (from the differential stress 270 MPa, point D) during the next 26 min. This indicates the growth of new microcracks. The strains of gauges C and E are more important than the other gauges because the final rupture plane was located throughout gauges C and E (Plate 1a and Figure 1a). Dynamic failure occurred at peak stress after a period of strain hardening.

The volume of JS sample was first decreased by 0.16%, similar to the intact sample, during the first 91 min of the experiment, and then began to slip when the differential stress was 260 MPa (S point). We did not observe some dilatancy during slip (at least absolute dilatancy of the total volume of the sample) as sometimes described [*Rudnicki and Chen*, 1988]. Note that there is no purely elastic (linear) volume changes, even at low stress, for the JS sample. A stress drop of 0.3 MPa was measured at the time of failure (in a time accuracy of 40 s). The slip, which cut the sample into two parts, was very clear since the behavior of the two strain gauges (A and B) glued on one part of the sample showed opposite behavior to the four other strain gauges glued on the other part of the sample (Figure 1b and plate 1b) (location of these strain gauges in regard to the slip being made after the experiment).

The final main rupture plane for JS sample was the same as the plane of the healed joint and was at an angle of ~20° compared to the axial stress direction, and for HS sample was at an angle ~32° (Figures 3 and 4). The shear and normal stresses resolved on a rupture plane inclined at an angle of α from the vertical are as follows [*Jaeger*, 1959; *Nicolas*, 1984]:

$$\tau = \frac{\sigma_1 - \sigma_3}{2} \sin(2\alpha)$$

$$\sigma_n = \frac{\sigma_1 + \sigma_3}{2} - \frac{\sigma_1 - \sigma_3}{2} \cos(2\alpha),$$

where σ_1 is the axial stress and σ_3 is the confining pressure.

At peak stress for HS sample the shear and the normal stresses on the fault inclined at the angle 32-34° from vertical are τ = 163.6 ± 2.8 MPa and σ_n = 146.3 ± 11.9 MPa. For JS sample the shear and normal stresses on the healed joint when slip occurred (at an angle 18-23° from vertical) are τ = 90.9 ± 9.3 MPa and σ_n = 74.5 ± 5.9 MPa. The friction $\mu = \tau / \sigma_n$ [*Byerlee*, 1978] on the rupture plane at peak stress is 1.12 ± 0.11 (HS sample) and on the healed joint when the slip occurred is 1.22 ± 0.22 (JS sample). These values are difficult to compare each other because the normal stresses are different. Shear stress versus normal stress for a large number of experiments (fracturation and sliding) on various materials has been reported and shows $\tau = 0.85\ \sigma_n$ for $\sigma_n < 200$ MPa [*Byerlee*, 1978; *Scholz*, 1990]. The friction deduced in our experiments (1.12 and 1.22) is higher than $\tau / \sigma_n = 0.85$ deduced by *Byerlee* [1978], higher than $\tau / \sigma_n = 0.86$ deduced from experiment of friction on blocks of granite at normal stress 70 MPa [*Dieterich*, 1972], and higher than $\tau / \sigma_n \sim 0.6$ deduced from experiment of gouge layer (quartz sand) sheared within Westerly granite surfaces in wet conditions at normal stress 100 MPa [*Marone et al.*, 1990]. We would expect a higher friction for the fracture experiment than for the sliding of the healed joint experiment at a given normal stress. This was observed when friction has been measured on Westerly granite in fracturing and sliding experiments [*Byerlee*, 1967]. For sliding experiments a law $\tau = 0.5 + 0.6\sigma_n$ was observed, leading to $\tau / \sigma_n = 0.5/\sigma_n + 0.6$ (τ and σ_n in kbar) equal to 1.27 when normal stress is 74.5 MPa (case of JS sample), which is closed to what we observed when slip occurred on the healed joint (friction equal 1.22 for JS sample). For fracturing experiments of Westerly granite the shear stress needed to fracture the sample was higher than for sliding (at a given normal stress) [*Byerlee*, 1967], so that for a normal stress of 146 MPa (HS sample) the friction would be 0.94 for sliding experiment and 1.55 for fracturing experiment. We deduced a friction of 1.12 for the experiment of fracturation (HS sample), which is lower than what was observed for Westerly granite fracturation but still higher than what was observed for Westerly granite sliding.

In summary, the HS sample fractured after an important volumetric change including dilatancy, with a high strength and an inferred friction coefficient 1.1, whereas the JS sample showed a slip (the joint itself fractures before it slides as it will be shown by acoustic emissions) after a compaction without showing significant dilatancy, with a lower strength, and an inferred friction coefficient 1.2. The presence of the healed joint weakened the strength of the sample.

4.2. *P* Wave Velocities

The values of *P* wave velocities were ~5.7-6.0 km/s for both samples. The evolution of vertical and horizontal *P* wave velocity during the deformation is detailed in Table 2. During the deformation of JS sample the velocities do not vary until the differential stress is 235 MPa, which is almost the end of the volume decrease of the sample. During the deformation of HS sample the vertical *P* wave velocity first increased from 5 to 5.96 km/s and then decreased when differential stress is ~130 MPa, which is well before the end of compaction, and then increased again. The horizontal *P* wave velocity first decreased or increased, depending on the orientation in the horizontal plane, and then decreased when the differential stress is ~130 MPa until the end of the experiment.

4.3. Acoustic Emissions

The cumulative number of AE events occurring during the experiments is shown in Figure 2. The total number of AE was

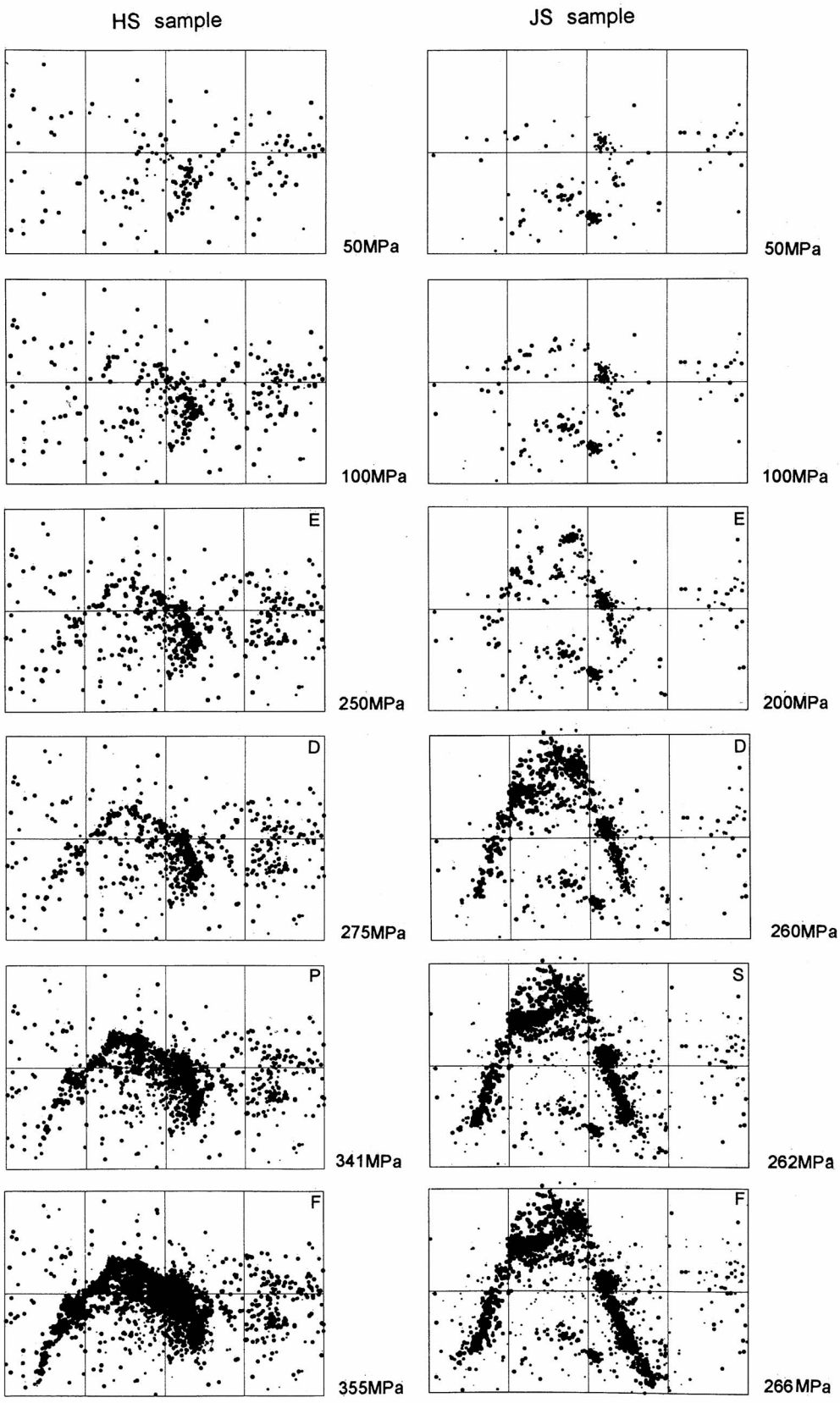

Figure 3. Evolution of the AE hypocenters location (lateral projection) during the triaxial compression at various differential stress values for HS sample and JS sample (letters refer to Figure 2). Length and circumference of the sample are 100 mm and 314 mm, respectively. The AE events of JS sample are distributed on the preexisting macroscopic joint.

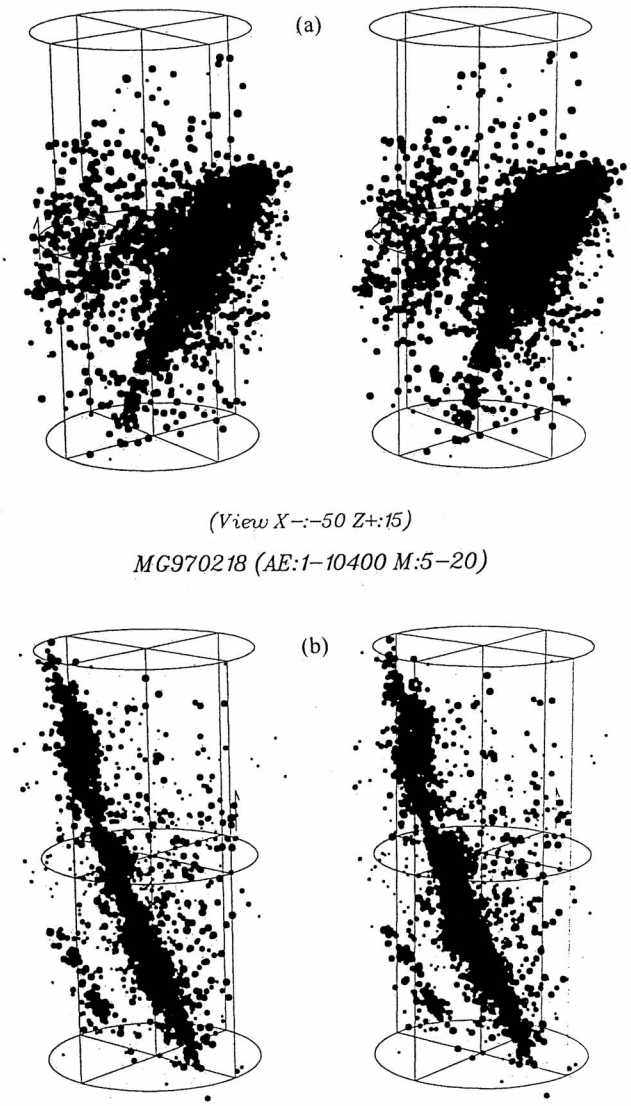

Figure 4. Stereographic projection of the AE hypocenters for (a) HS and (b) JS samples. Length and diameter of the sample are 100 mm and 50 mm, respectively.

11,207 and 18,411 for HS and JS samples, respectively. AE activity was observed during the linear elastic phase (up to E point). The AE rate was roughly constant up to 56% (200 MPa) and 72% (200 MPa) of the strength for HS and JS samples, with an AE rate larger at the very beginning of the compression for HS sample compared to JS sample. The end of the constant AE rate for HS sample coincides with the end of the linearity between differential stress and volumetric strain (56%). At the end of the compression phase (point D) both samples showed a decrease in volume of 0.16%. For HS sample, AE events were 14% (~1600 AE) of the total amount of events, and the differential stress was 275 MPa meaning 77% of the strength. For JS sample, just before the slip occurred, AE events were 13-14% (~2500) of the total amount of AE events, and the differential stress was 253-257 MPa meaning 91-92% of the strength. At this point the behavior of both samples is quite similar, except that the JS sample exhibits ~1.6 times more AE events in absolute value. It would mean that the deformation at this stage induces more microcracks or slipping in the sample containing the joint than in the intact sample, and particularly within the healed joint.

The AE hypocenter locations (deduced from a number of sensors between 5 and 20) are shown in Figure 3 when the differential stress was 50 MPa and then 100 MPa and the final rupture plane is not yet localized. Another plot of the hypocenters when the differential stress was 250 MPa for HS sample and 200 MPa for JS sample, meaning the end of elastic phase (point E), shows the progression of the localization of the hypocenters on the final rupture plane. The final plane of rupture can already be seen in both experiments. Note that the AE distribution is distributed throughout the volume for HS sample but is planar on the preexisting joint for JS sample. The localization of the hypocenters at the end of the compression phase at 275 MPa and 260 MPa for HS and JS samples is shown as point D. At this point it is clearly shown that the future plane of rupture is already well localized before any dilatancy. Finally, the hypocenter locations are shown near the rupture (95% and 99% of strength, points P and F) (Figures 2 and 3) for HS sample and just at the slip and after the slip for JS sample (points S and F).

5. Discussion

Some observations showing that the start of AE activity corresponds to the onset of dilatancy, defined as the beginning of the nonlinear part of the axial stress-volumetric strain curve (volume increases relative to elastic changes), have been reported (*Scholz* [1968a] and *Meredith et al.* [1990] for a granite sample and *Takahashi and Abé* [1987]). On the other hand, AE activity prior to the onset of dilatancy has also been observed [*Scholz*, 1968b; *Kurita and Fujii*, 1979; *Gowd*, 1980; *Ohnaka and Mogi*, 1982; *Fonseka et al.*, 1985; *Meredith at al.*, 1990; *Kusunose et*

Table 2. *P* Wave Velocity Values During the Deformation for HS and JS Samples[a]

Differential Stress, MPa	P_V, km/s	P_{H1}, km/s	P_{H2}, km/s
	HS Sample		
0	5.00	5.26	5.49
9.9	5.66	6.25	5.95
34.9	5.84	6.10	5.99
59.9	5.88	5.99	6.02
84.9	5.95	6.02	6.10
109.9	5.96	6.17	6.02
159.8	5.95	5.99	6.02
209.8	5.88	6.02	5.95
259.7	5.95	5.88	5.95
314.7	6.04	5.65	5.75
	JS Sample		
0	5.86	5.70	5.70
39.9	5.90	5.70	5.70
59.9	5.97	5.70	5.70
209.8	5.97	5.70	5.70
234.7	6.00	5.50	5.50

[a] P_V is the vertical *P* wave velocity (maximum error of ±0.5% and ±0.35% for HS and JS samples, respectively), P_{H1} and P_{H2} are the horizontal *P* wave velocity (maximum error of ±0.2% and ±0.1% for HS and JS samples, respectively).

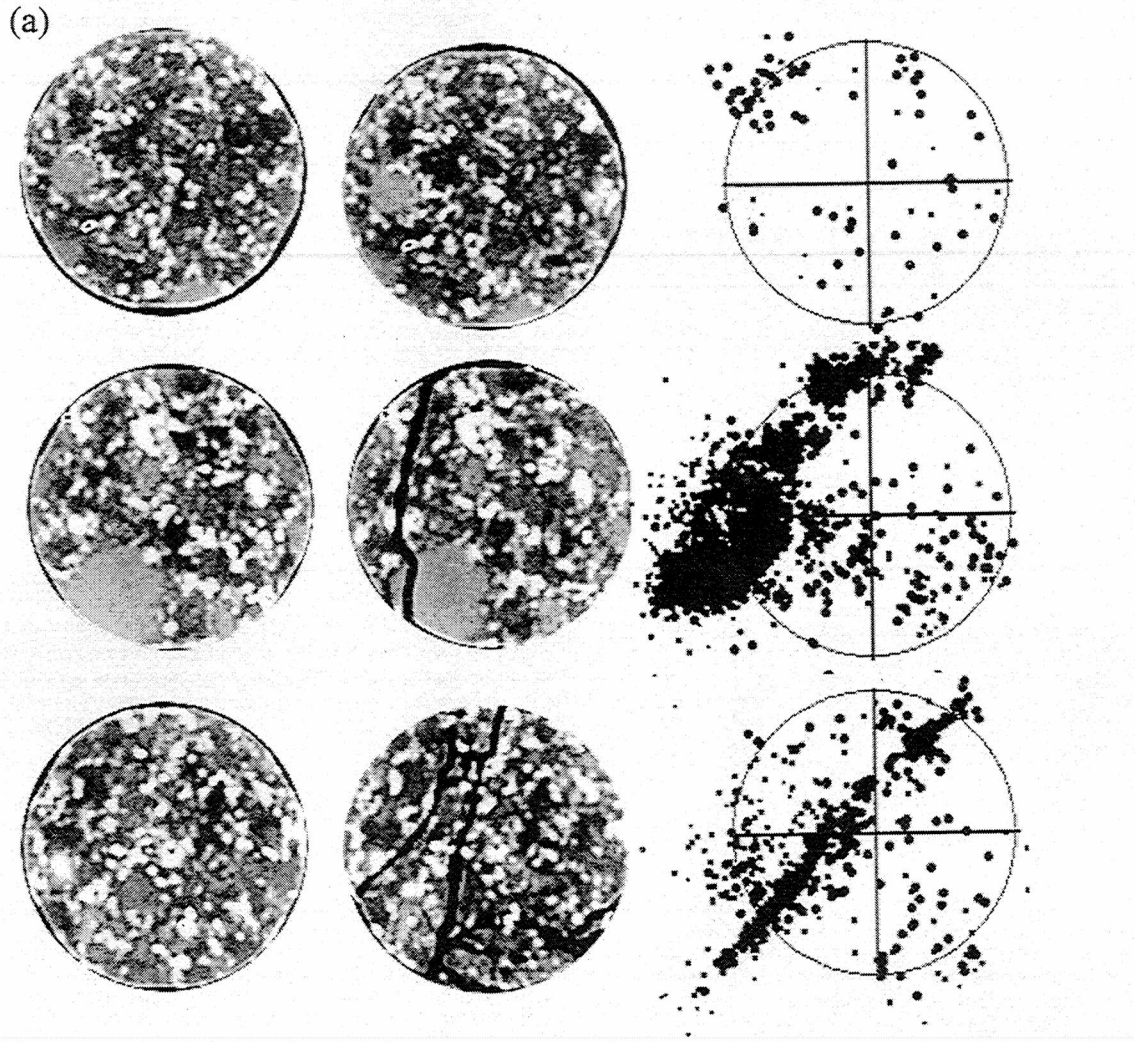

Figure 5. Scanner X images of three cross sections of (a) HS and (b) JS samples, (left) before the experiment, (middle) after the rupture, and (right) projections of the AE hypocenters. Diameter of the sample is 50 mm. Cross sections at the top and bottom are at 30 mm from the ends of the sample, and cross section in the middle corresponds to the middle of the sample. Diameter of cross sections is ~50 mm. Large grains are feldspar. Large black channel is the rupture.

al., 1991]. Such activity is associated with initial closure under compression of favorably oriented cracks already present, together with sliding of crack faces. Compaction-induced AE has been interpreted as due to friction between interlocking grains, the breaking of partially healed portions and asperities on preexisting crack surfaces during compaction, and closure of preexisting cracks under stress, at large angles to the compression axis [*Gowd*, 1980; *Meredith et al.*, 1990; *Ohnaka and Mogi*, 1982]. The permanent AE activity during our experiments, meaning the existence of AE activity well before the dilatancy, suggests that even a low-porosity rock such as a granite cannot be purely elastic in the linear part of the stress-strain curve because the generation of AE involves locally inelastic processes [*Ohnaka and Mogi*, 1982].

Then AE activity is usually found to increase exponentially when the deviatoric stress is increased [*Scholz*, 1968b; *Kurita and Fujii*, 1979; *Gowd*, 1980; *Ohnaka and Mogi*, 1982; *Meredith et al.*, 1990]. This increase in acoustic activity is usually attributed to atomic bond breaking and the creation of new stress-induced cracks that are successively produced [*Sondergeld and Estey*, 1981]. Then the rapid acceleration of AE activity before and during failure is usually explained by the growth process of large cracks and by their coalescence.

In some case, an apparent seismic quiescence is observed. *Liakopoulou-Morris et al.* [1994] measured the AE during the fault nucleation and sliding and strengthening of a sandstone sample under constant strain rate. They showed that during the fault nucleation the AE event rate increased very slowly in the linear quasi-elastic phase and accelerated markedly in the strain-hardening phase, consistent with dilatant microcrack growth. During the period of postpeak strain softening, a decrease in AE events was observed, implying an apparent seismic quiescence. During the sliding phase, characterized by a relatively constant differential stress, the variations in AE rate were much smaller than in the nucleation phase. In the case of HS sample, no stress decrease was measured, as can be observed in postpeak strain softening, implying coalescence of existing microcracks to form a throughgoing fault. In the case of JS sample the slip was different from stable sliding under quasi-constant differential stress usually observed after postpeak strain softening and

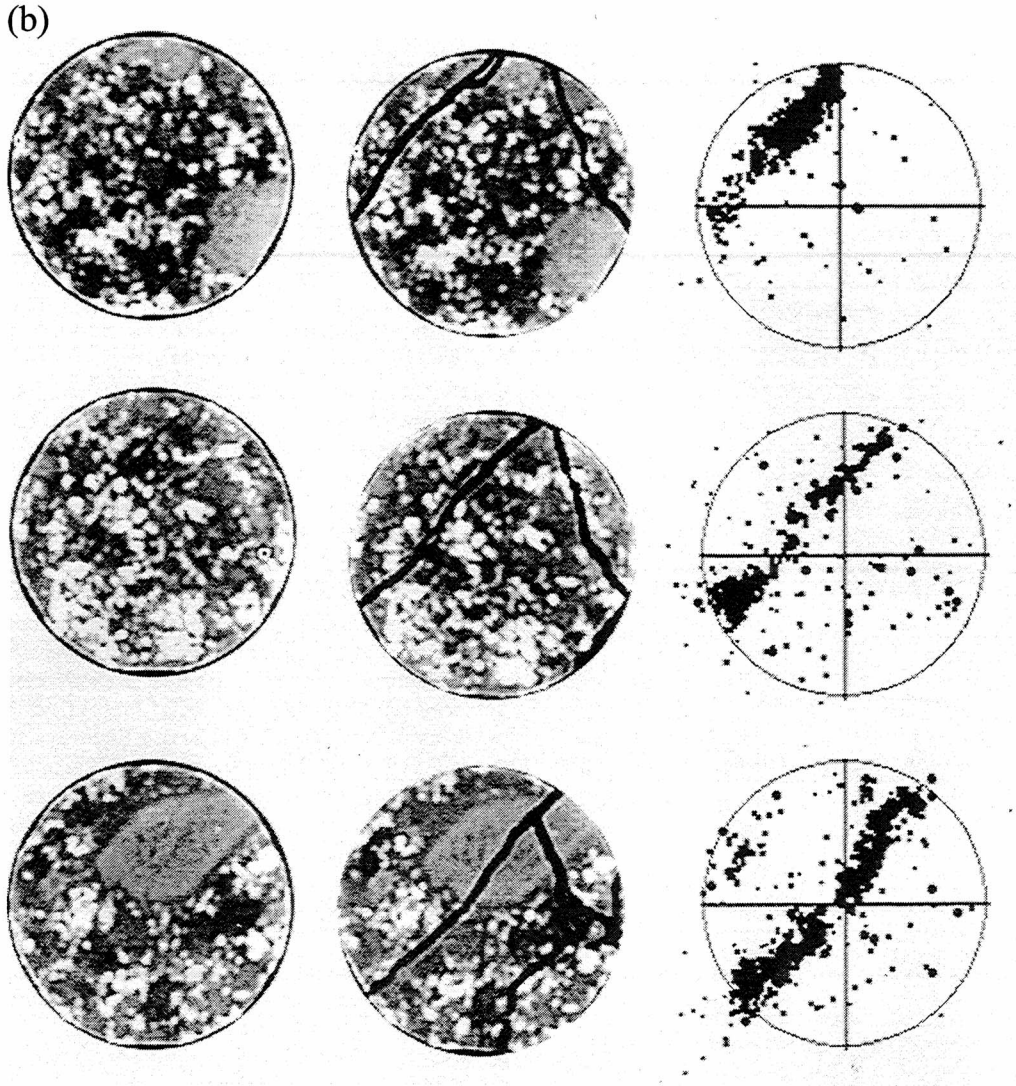

Figure 5. (continued)

unstable dynamic failure [*Gowd*, 1980; *Meredith et al.*, 1990; *Liakoupoulou-Morris et al.*, 1994; *Baddari et al.*, 1996]. The slip of the healed joint of JS sample occurred under a drop of differential stress of ~0.3 MPa. *Meredith et al.* [1990] noted that only when a period of strain softening preceded dynamic rupture, was AE rate flattenned and decreased to a period of apparent seismic quiescence. Since a post peak strain softening was not observed in our experiments, the absence of a kind of quiescence is not in contradiction with these earlier observations.

The early localization of the main final rupture plane, well before dilatancy (see points E and D in Figures 2 and 3), deduced from the hypocenters of the AE measurements in our experiments of fracturation in one hand, and of slipping in the other hand, differs from the usual inference from previous studies [e.g., *Scholz*, 1968c]. Indeed, during a cyclic loading experiment on Oshima granite [*Satoh et al.*, 1990] the AE hypocenters did not concentrate preferentially on the ultimate fracture planes, but they concentrated around a part of the main fault plane prior to the ultimate fracture. The sample fractured in a brittle manner, and there was no postpeak stage. The AE hypocenters formed a number of clusters in which hypocenters aligned in the directions parrallel or conjugate to the main fault. *Satoh et al.* [1990] concluded that the most plausible mechanisms of fault development was shear linking of an axial crack array [*Wong*, 1982]. In triaxial compression experiments on granite and sandstone samples by controlling axial stress to maintain constant AE rate, the fault growth and shear fracture have been followed quasi-statically [*Lockner et al.*, 1991, 1992]. In that case the postpeak weakening curve corresponds to propagation of the macroscopic fault plane across the sample, and microcracking, as determined by AE locations, remained uniformly distributed in the central portion of the granite samples until after peak stress. The low and uniformly distributed events reflected homogeneous microcracking during the loading phase. There was no obvious precursor in AE event locations (meaning clustering of AE) to indicate the position of the nucleation zone, so that it was concluded that microcracks were sparse and damage remained diffuse until near peak stress. Note that in sandstone samples, significant AE was occurring by ~40% of peak stress and was interpreted as indicating the presence of a weak zone. In another experiment of symmetric loading of granite sample the clustering of events was also found only after the failure [*Zang et al.*, 1998]

When some precursor localization (meaning precursor

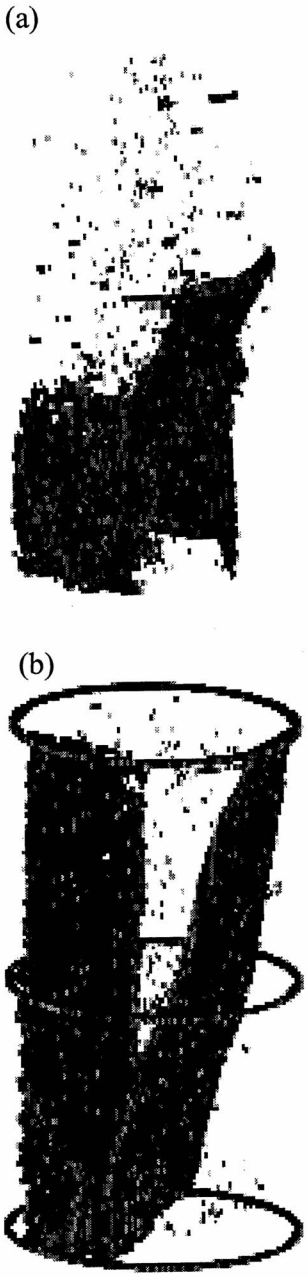

Figure 6. Three-dimensional scanner X image of the fracture planes of samples (a) HS and (b) JS. Length and diameter of the sample are 100 mm and 50 mm, respectively.

behavior of AE) is observed, it is usually deduced that it is induced by a weak zone. For example, during the uniaxial cycling of a Westerly granite sample, strong spatial clustering of hypocenters has been observed and was thought to be induced by nonhomogeneous dilatancy development [*Sondergeld and Estey*, 1981]. During another triaxial creep experiment on amphibolite [*Satoh et al.*, 1996], precursory localization of AE hypocenters was observed. This precursory nucleation and development of a macroscopic fracture plane was induced by a preexisting macroscopic defect. Moreover, no significant precursory localization of AE hypocenters on the final fracture plane before failure has been reported in rock sample free of preexisting macroscopic defects. In another experiment, when deforming a granite sample under uniaxial compression with a constant stress rate, *Shah and Labuz* [1995] observed that the microseismic activity was more or less uniformly distributed on the sample until ~85% of the maximum loading, when concentration of AE hypocenters was observed.

In both cases of HS sample and JS sample the precursory localization of the final rupture plane is clearly observed as soon as the end of the pseudo-elastic phase (E point in Figure 2) and well before the dilatancy (D point), meaning that the damage does not remain diffuse and uniformly distributed. In the case of JS sample the healed joint controls the stress heterogeneity and therefore the final rupture, and the AE distribution is planar. In the case of HS sample the heterogeneity in grain size controls the stress heterogeneity and therefore the rupture nucleation, and the AE distribution is volumic distributed.

Scanner X images of the cross sections of our granite samples have been performed, before and after the experiment (Figure 5), and have been rebuilded in three dimensions (Figure 6). Minerals and grain sizes of this granite are very different, from 1 mm to 3 cm. Large grains in Figure 5 are feldspar. This inhomogeneity may be a main difference of our experiment compared to other samples used in previous experiments. It is likely that the grain-scale inhomogeneity and differences in elastic moduli between minerals can influence the local stress field significantly. Geometry of the fracture can be seen in Figure 6 and corresponds to the AE distribution plotted in Figure 4. For JS sample the plane indicated by AE location was formed during the deformation of the rock. The other plane (Figure 6b) was formed just before the final rock fracture in the very short time or at the same time of the final fracture. That is why this plane is not accompanied by AE and its location is very close (and parallel) to the surface.

An interpretation of fault growth, based on optical and scanning electron microscope observation of Berea sandstone samples retrieved at different stages of deformation, has been proposed by *Menendez et al.* [1996]. They observed that in the brittle regime, shear localization does not develop until the postfailure stage and that very little intragranular cracking occurred before the peak stress was attained. As stress concentrations at grain contacts are not sufficient to initiate stress-induced extensile cracking, they proposed that the local *shear* stress concentrations are sufficiently high to cause the grains to move relative to one another by rotation and slip. This intergranular cracking, probably related to the shear rupture of cemented grain contacts, could also induce dilatancy and AE activity in the prefailure stage. Then, in the close vicinity of the peak stress, intragranular fractures develop in isolated clusters, and the coalescence of a high density of clusters results in shear localization [*Menendez et al.*, 1996]. Note that this study was performed on Berea sandstone of relative high porosity compared to the low-porosity rock granite used here.

Whatever is the exact mechanism involved in the fracturing (HS sample) and in the slipping (JS sample) of our granite samples, the acoustic emission hypocenters are localized on the final rupture plane in the early stage of deformation process, involving locally inelastic processes. It is likely that not only initial closure of favorably oriented cracks but also breaking of partially cemented grains contacts or sliping between grains may occur in the pseudoelastic phase, distributed on the final rupture plane, where the shear stress seems to be concentred. This behavior is observed in both cases where stress heterogeneity and

rupture nucleation are controlled by (1) medium-scale heterogeneity at the grain scale (HS sample) or (2) macroscopic heterogeneity in the form of a preexisting healed joint (JS sample).

6. Conclusion

Localization of the rupture in one experiment and localization of the slip of a preexisting macroscopic healed joint in the other experiment, on the granite from Mayet de Montagne, have been observed in the early stage of deformation, whatever controls the stress heterogeneity and rupture nucleation: (1) medium-scale heterogeneity at the grain scale (HS sample) or (2) macroscopic heterogeneity in the form of a preexisting healed joint (JS sample). Since the early localization of the rupture was not reported in previous experiments in the literature, using other samples with a smaller grain size to sample ratio, a comparison should be made on different granite samples with various grain sizes and various degrees of heterogeneity, using the same technology, in order to understand the different behaviors of the different granite samples.

Acknowledgments. F. Cornet (IPGParis) is thanked for providing the granite samples from Mayet de Montagne (France). The initial project of these experiments has benefitied from discussions with M. Zamora and J.-P. Pozzi (ENS Paris). We thank Pierre Bésuelle for fruitful discussions. This paper was greatly improved by the associate editor Ian Main. We thank S. Yoshida for his review. This research is a CNRS-INSU-PNRN contribution 258 (Thème risques sismiques) and was partly supported by CNRS and ANDRA through the GdR FORPRO (Research Action 99-VIII) and corresponds to the GdR FORPRO contribution 2000/17 A.

References

Ashby, M.F., and S.D. Hallam, The failure of brittle solids containing small cracks under compressive stress states, *Acta Metall., 34*, 497-510, 1986.

Ashby, M.F., and C.G. Sammis, The damage mechanics of brittle solids in compression, *Pure Appl. Geophys., 133*, 489-521, 1990.

Baddari, K., G. A. Sobolev, and A.D. Frolov, Similarity in seismic precursors at different scales, *C. R. Acad. Sci. Paris, Ser. IIa, 323*, 755-762, 1996.

Brace, W.F., B.W. Paulding, and C. Scholz, Dilatancy in the fracture of crystalline rocks, *J. Geophys. Res., 71*, 3939-3953, 1966.

Byerlee, J., Frictional characteristics of granite under high confining pressure, *J. Geophys. Res., 72*, 3639-3647, 1967.

Byerlee, J., Friction of rocks, *Pure Appl. Geophys., 116*, 615-626, 1978.

Clavaud, J.B., M. Zamora, F. Cornet, G. Michard, P. Zuddas, J.M. Boffa, and J.P. Hulin, Permeability change by dissolution or precipitation effects in granite with a single fracture, paper presented at XXV General Assembly, Eur. Geophys. Soc., Nice, France, 2000.

Costin, L.S., A microcrack model for the deformation and failure of brittle rock, *J. Geophys. Res., 88*, 9485-9492, 1983.

Dieterich, J.H., Time-dependent friction in rocks, *J. Geophys. Res., 77*, 3690-3697, 1972.

Fonseka, G.M., S.A.F. Murell, and P. Barnes, Scanning electron microscope and acoustic emission studies of crack development in rocks, *Int. J. Rock Mech. Min. Sci. Geomech. Abstr., 22*, 273-289, 1985.

Gowd, T.N., Factors affecting the acoustic emission response of triaxially compressed rock, *Int. J. Rock Mech. Min. Sci. Geomech. Abstr., 17*, 219-223, 1980.

Jaeger, J.C., The frictional properties of joints in rock, *Geofis. Pura Appl., 43*, 148-158, 1959.

Kurita, K., and N. Fujii, Stress memory of crystalline rocks in acoustic emission, *Geophys. Res. Lett., 6*, 9-12, 1979.

Kusunose, K, X. Lei, O. Nishizawa, and T. Satoh, Effect of grain size on fractal structure of acoustic emission hypocenter distribution in granitic rock, *Phys. Earth Planet. Inter., 67*, 194-199, 1991.

Lei, X., O. Nishizawa, T. Satoh, and K. Kusunose, An AE data processing program for windows (in Japanese with English abstract), *Bull. Geol. Surv. Jpn., 48*, 447-457, 1997.

Lei, X., K. Kusunose, M.V.M.S. Rao, O. Nishizawa, and T. Satoh, Quasi-static fault growth and cracking in homogeneous triaxial compression using acoustic emission monitoring, *J. Geophys. Res., 105*, 6127-6139, 2000.

Liakopoulou-Morris, F., I.G. Main, B.R. Crawford, and B.G.D. Smart, Microseimic properties of a homogeneous sandstone during fault nucleation and frictional sliding, *Geophys. J. Int., 119*, 219-230, 1994.

Lockner, D., The role of Acoustic emission in the study of rock fracture, *Int. J. Rock Mech. Min. Sci. Geomech. Abstr., 30*, 883-899, 1993.

Lockner, D.A., and J.D. Byerlee, How geometrical constraints contribute to the weakness of mature faults, *Nature, 363*, 250-252, 1993.

Lockner, D.A., J.D. Byerlee, V. Kuksenko, A. Ponomarev, and A Sidorin, Quasi-static fault growth and shear fracture energy in granite, *Nature, 350*, 39-42, 1991.

Lockner, D.A., J.D. Byerlee, V. Kuksenko, A. Ponomarev, and A. Sidorin, Observations of quasistatic fault growth from acoustic emissions, in *Fault Mechanics and Transport Properties of Rocks*, edited by B. Evans and T.-F. Wong, pp. 3-29, Academic, San Diego, Calif., 1992.

Main, I.G., A modified Griffith criterion for the evolution of damage with a fractal distribution of crack lengths: Application to seismic event rates and *b*-values, *Geophys. J. Int., 107*, 353-362, 1991.

Marone, C., C. B. Raleigh, and C.H. Scholz, Frictional behavior and constitutive modeling of simulated fault gouge, *J. Geophys. Res., 95*, 7007-7025, 1990.

Masuda, K., O. Nishizawa, K. Kusunose, T. Satoh, M. Takahashi, and R.L. Kranz, Positive feedback fracture process induced by nonuniform high-pressure water flow in dilatant granite, *J. Geophys. Res., 95*, 21,583-21,592, 1990.

Menendez, B., W. Zhu, and T.-F. Wong, Micromechanics of brittle faulting and cataclastic flow in Berea sandstone, *J. Struct. Geol., 18*, 1-16, 1996.

Meredith, P.G., I.G. Main, and C. Jones, Temporal variations in seismicity during quasi-static and dynamic rock failure, *Tectonophysics, 175*, 249-268, 1990.

Moore, D.E., and D.A. Lockner, The role of microcracking in shear-fracture propagation in granite, *J. Struct. Geol., 17*, 95-114, 1995.

Nemat-Nasser, S., and H. Horii, Compression-induced nonplanar crack extension with application to splitting, exfoliation, and rockburst, *J. Geophys. Res., 87*, 6805-6821, 1982.

Nicolas, A., *Principes de Tectonique*, Masson, Paris, 1984.

Nishizawa, O., New multi-wire type and co-axial type feedthroughs for an oil pressure-medium vessel (in Japanese with English abstract), *Bull. Geol. Surv. Jpn., 48*, 431-438, 1997.

Ohnaka, M., and K. Mogi, Frequency characteristics of acoustic emissions in rocks under triaxial compression and its relation to the fracturing process to failure, *J. Geophys. Res., 87*, 3873-3884, 1982.

Reches, Z., and D.A. Lockner, Nucleation and growth of faults in brittle rocks, *J. Geophys. Res., 99*, 18,159-18,173, 1994.

Rudnicki, J.W., and C.H. Chen, Stabilization of rapid frictional slip on a weakening fault by dilatant hardening, *J. Geophys. Res., 93*, 4745-4757, 1988.

Satoh, T., and O. Nishizawa, A high speed, multi-channel waveform recording system for AE measurement (in Japanese with English abstract), *Bull. Geol. Surv. Jpn., 48*, 439-446, 1997,

Satoh, T., K. Kusunose, and O. Nishizawa, A minicomputer system for measuring and processing AE waveforms-High speed digital recording and automatic hypocenter determination (in Japanese with English abstract), *Bull. Geol. Surv. Jpn., 38*, 295-303, 1987.

Satoh, T., O. Nishizawa, and K. Kusunose, Fault development in Oshima granite under triaxial compression inferred from hypocenter distribution and focal mechanism of acoustic emission, *Tôhoku Geophys. J., Sci. Rep. Tôhoku Univ., Ser. 5, 33*, 241-250, 1990.

Satoh, T., K. Shivakumar, O. Nishizawa, and K. Kusunose, Precursory localization and development of microfractures along the ultimate fracture plane in amphibolite under triaxial creep, *Geophys. Res. Lett., 23*, 865-868, 1996.

Scholz, C.H., The frequency-magnitude relation of microfracturing in rock and its relation to earthquakes, *Bull. Seismol. Soc. Am., 58*, 399-415, 1968a.

Scholz, C.H., Microfracturing and the inelastic defomation of rock in compression, *J. Geophys. Res., 73*, 1417-1432, 1968b.

Scholz, C.H., Experimental study of the fracturing process in brittle rock, *J. Geophys. Res.*, *73*, 1447-1454, 1968c.

Scholz, C. H., *The Mechanisms of Earthquakes and Faulting*, pp. 53-66, Cambridge Univ. Press, New York, 1990.

Shah, K.R., and J.F. Labuz, Damage mechanisms in stressed rock from acoustic emission, *J. Geophys. Res.*, *100*, 15,527-15,539, 1995.

Sondergeld, C.H., and L.H. Estey, Acoustic emission study of microfracturing during the cyclic loading of Westerly granite, *J. Geophys. Res.*, *86*, 2915-2924, 1981.

Takahashi, H., and H. Abé, Fracture mechanics applied to hot, dry rock geothermal energy, in *Fracture Mechanics of Rock*, edited by B.K. Atkinson, pp. 254-257, Academic, San Diego, Calif., 1987.

Tapponier, P., and W.F. Brace, Development of stress-Induced microcracks in Westerly granite, *Int. J. Rock Mech. Min. Sci. Geomech. Abstr.*, *13*, 103-112, 1976.

Wong, T.-F., Micromechanics of faulting in Westerly granite, *Int. J. Rock Mech. Min. Sci. Geomech. Abstr.*, *19*, 49-64, 1982.

Yokota, T., S. Zhou, M. Mizoue, and I. Nakamura, An automatic measurement of arrival time of seismic waves and its application to an on-line processing system (in Japanese with English abstract), *Bull. Earthquake Res. Inst. Univ. Tokyo*, *55*, 449-484, 1981.

Zang, A., F.C. Wagner, S. Stanchits, G. Dresen, R. Andresen, and M.A., Haidekker, Source analysis of acoustic emissions in Aue granite cores under symmetric and asymmetric compressive loads, *Geophys. J. Int.*, 135, 1113-1130, 1998.

L. Jouniaux, Laboratoire de Géologie de l'Ecole Normale Supérieure de Paris, UMR 8538, 75231 Paris Cedex 05, France. (jouniaux@geologie.ens.fr)

K. Kusunose, X. Lei, K. Masuda, and O. Nishizawa, Geological Survey of Japan, Higashi 1-1-3, Tsukuba, Ibaraki 305, Japan. (kin@gsj.go.jp; lei@gsj.go.jp; masuda@gsj.go.jp; osamu@gsjkouji.gsj.go.jp)

L. Liu and W. Ma, Institute of Geology and Laboratory of Tectonophysics, China Seismological Bureau, Beijing, China.

(Received February 28, 2000; revised October 25, 2000;
accepted November 6, 2000.)